Interbasin groundwater flow: Characterization, role of karst areas, impact on annual water balance and flood processes

Martin Le Mesnil, Jean-Baptiste Charlier, Roger Moussa, Yvan Caballero, Nathalie Dörfliger

Interbasin Groundwater Flow: Characterization, Role of karst areas, Impact on annual water balance and flood processes

Martin Le Mesnil* (1,2), Jean-Baptiste Charlier (1), Roger Moussa (2), Yvan Caballero (1), Nathalie Dörfliger (3)

(1) BRGM, Univ. Montpellier, Montpellier, France

(2) LISAH, Univ. Montpellier, INRA, IRD, Montpellier SupAgro, Montpellier, France

(3) BRGM, F-45060 Orléans, France

* Corresponding author e-mail: martin.le-mesnil@inra.fr

Introduction

Catchments are generally considered as self-contained hydrological units, without exchange with their neighbours. In this way, traditional water-balance methods allow estimating the not-so-easily measured evapotranspiration term (E) by measuring two other ones (rainfall P and streamflow Q). Among the earliest and most influential of these methods can be cited the works of Budyko [1974] and L'vovich [1979]. L'vovich [1979] introduced the idea of two-stage annual water-balance partitioning at the catchment scale, suggesting that, in a first step, precipitation is partitioned into surface runoff and wetting, and that subsequently the wetting is partitioned into evapotranspiration and underground flow. This kind of approach allows convenient regionalization of water-balances. For example, Ponce and Shetty [1995] proposed mathematical formulations for the L'Vovich concept, and Sivapalan et al. [2011] adapted them to numerous catchments in the USA. Such water-balance theories are based on the strong assumption that every catchment is "conservative", by considering that P is the sum of

Q and E. For this reason, authors using this framework often explicitly discard “non-conservative” catchments [e.g. Laaha and Blöschl, 2006]. However, hardly or not measurable flows can noticeably influence water balance, such as water abstraction by pumping [Ladouche et al., 2014; Charlier et al., 2015a], overbank flow phenomena [Bates and De Roo, 2000; Moussa and Bocquillon, 2009], or interbasin groundwater flow (IGF) [Eakin, 1966].

Among these, IGF is certainly the most common and important. As an example, the recent publication of Fan [2019] gathers evidence from mass balance that catchments across the globe can exhibit leakages through their topographic divides. IGF has been shown to occur in sedimentary, volcanic or karst-system catchments [Genereux et al., 2002, 2005; Schaller and Fan, 2009; Charlier et al., 2011]. Even if not directly measurable, IGF can be identified with hydrogeochemical methods based on major dissolved elements, isotopes, electrical conductivity and water temperature monitoring [Genereux and Jordan, 2006; Carrillo-Rivera et al., 1996, 2000] , or through hydrogeological studies of groundwater flow paths [Thyne et al., 1999]. Conceptually, IGFs reflect the non-superposition of topographic and hydrogeological catchment areas: they generally involve a “gaining” catchment with its *hydrogeological* boundaries extending inside the *topographic* boundaries of a neighbouring “losing” catchment. As such, a water-budget approach can also assume the possible influence of IGF. As an example, Pellicer-Martínez and Martínez-Paz [2014] applied a semi-distributed lumped model for quantifying IGFs in a Spanish catchment. In France, Andréassian and Perrin [2012] plotted 2300 catchments in a Budyko-type diagram and showed that over 20% of them fall outside the conservative zone defined by $P = Q+E$, with $0<E<E0$, E0 being the potential evapotranspiration. Bouaziz et al. [2018] also linked IGF to Budyko diagrams in the Meuse basin, with similar results.

Some studies [Le Moine et al., 2007; Lebecherel et al., 2013; Fan, 2019], noticed that many non-conservative catchments lie in karst areas, without further investigating this issue. Indeed, IGFs are very common in karst catchments, due to their high infiltration capacity promoting groundwater flow, and to the non-coincidence of topographic and hydrogeological catchment boundaries. Karstification is the product of carbonate-rock dissolution, enlarging fissures and creating voids that considerably reduce drainage density—going even as far as an absent drainage network with so-called dry valleys—and favours groundwater flow through conduit networks [Bakalowicz, 2005]. Consequently, different loss and gain processes affect streamflow where rivers cross karst areas [Bailly-Comte et al., 2009; Charlier et al., 2015b, 2019]. Such processes are subject to fluctuations, depending upon karstification degree, water-table level changes, and surface-water/groundwater interactions [Bailly-Comte et al., 2009; Charlier et al., 2019]. For instance, an *estavelle* (typical karst orifice) can serve as a sinkhole or a spring, depending on karst aquifer saturation [Lopez-Chicano et al., 2002; Mayaud et al., 2019]. Moreover, IGF affects both quick- and slow-flow components (storm flow and baseflow). For example, Charlier et al. [2015b] showed the important role of karst springs on flood flow in the Tarn River, Maréchal et al. [2008] showed that groundwater may represent 60% of the river flow during a flood recession, and Charlier et al. [2019] showed the importance of river losses on attenuating the flood component due to infiltration in karst. Accounting for IGF in water balance approaches is thus essential in karst catchments, which cover around 30% of the European land surface [Chen et al., 2017].

The aim of this paper is to develop a framework to apply water balances to a wide range of natural catchments, including non-conservative ones, such as those located in karst areas that are prone to IGF. To estimate this additional IGF component, actual evapotranspiration is assessed using independent data, regardless of rainfall-runoff relationships. IGF is considered as the difference between catchments input (P) and outputs (Q and E). This equivalence assumes that IGF is the only source of non-conservativeness of the water balance. We adopted this assumption here as we also assumed that anthropogenic influence (withdrawals) and overbank phenomena can be neglected compared to IGF in most large- to medium-scale catchments (>50 km²), and because time series spanning several years allow neglecting the interannual water-volume variation.

In this study, we thus drew up annual water balances including IGF for conservative and non-conservative catchments having outcrops of karst formations. Knowing that IGF affects streams during both high- and low-flow stages [Maréchal et al., 2008; Charlier et al., 2015b], an adapted model integrating hydrograph decomposition was needed. To this end, we developed an annual L'vovich model, adapted to non-conservative catchments. In order to obtain a better resolution of the spatial variability, we applied it to the scale of the river reaches and their corresponding elementary catchments. This allowed us identifying their hydrological flood response and linking it to easily estimated geomorphological parameters, in order to assess the transferability of our results to ungauged basins. We applied this approach to 120 elementary catchments, having an average area of 100-500 km². The three main original features of our work are that annual water-balance methods: i) are applied to non-conservative catchments, ii) include a hydrograph decomposition that allows describing the flood catchment response, and iii) are performed at the elementary catchment scale and linked to geomorphological parameters.

1 Methodology

1.1 Adaptation of the L'vovich water-balance method to account for Interbasin Groundwater Flow

1.1.1 Initial L'vovich water balance for conservative catchments

L'vovich [1979] introduced the idea of a two-stage annual water-balance partitioning at the catchment scale, suggesting that, as a first step, precipitation (P) is partitioned into surface runoff (S) and wetting (W), and that in a second step W is further partitioned into evapotranspiration (E) and underground flow (U). This theory, shown on Figure 1A, allows writing the following equations, corresponding to the two stages of precipitation partitioning, applicable at the annual scale (Eqs. 1 and 2), and to baseflow separation (Eq. 3):

$$P = W + S \qquad (1)$$

$$W = E + U \qquad (2)$$

$$Q = S + U \qquad (3)$$

Of these terms, P and Q are measured, and S and U are obtained by hydrograph separation on daily-data time series. Equations 1 and 2 provide annual values of W and E, respectively. This water-balance method can be done through simple graphical hydrograph decomposition, as well as with numerical models [e.g. Eckhardt, 2005; Tang and Carey, 2017]. More details on this aspect are given in section 1.1.3. This theory implies that every catchment lies on a watertight substratum (without IGF), and that annual precipitation is completely recovered when adding annual evapotranspiration and streamflow (Eq. 4).

$$P = Q + E \qquad (4)$$

1.1.2 Adapted L'vovich water balance for non-conservative catchments

In order to write a consistent water balance for all catchments, including non-conservative ones, we propose to account for the annual IGF component, as shown in Equation 5. To account for I, independent data sets are necessary to assess actual evapotranspiration E* (section 1.1.4).

$$I = P - Q - E^* \qquad (5)$$

The obtained I values can be positive, representing an IGF outflow, or negative for IGF inflow (Fig. 1B). The annual calculation of IGF allows separating the measured streamflow Q into catchment runoff production (Q*) and groundwater gains or losses I. Q* is obtained by operating an IGF compensation on Q, as follows:

$$Q^* = Q + I \qquad (6)$$

As Equation 5 is not applicable at a daily time step (due to the transfer time of P in soil or canopy before contributing to E or Q), I is calculated annually. Despite some residence times in matrix ranging from 100 to 300 days, this assessment remains reliable, the final IGF value being a pluri-annual mean obtained from time series of around 10 hydrological years (see Table 1). This allows redressing annual water balances by capturing the potential water storing and releasing over hydrological years. Since preliminary results show that both S and U are affected by I, IGF is compensated for both S and U, obtained with the initial L'vovich model. The new variables, S* and U*, are representative of the surface quick runoff and slow underground runoff before IGF influence, whereas S and U are the respective quick and slow components of a signal composed of catchment runoff and the associated IGF (Fig. 1B).

[Figure 1]

Since IGF affects surface- and underground-runoff in complementary volumes that vary depending on the catchments, a site-dependent α coefficient is defined for describing the distribution of the IGF impact on both streamflow components (Eqs. 7 and 8).

$$S^* = S + I \cdot \alpha \qquad (7)$$

$$U^* = U + I \cdot (1 - \alpha) \qquad (8)$$

If IGF is the main cause of non-conservativeness, the water balances calculated with S* and U* should be conservative. Thus, for each catchment, α is calibrated in order to minimize the number of non-conservative annual water balances on the available data time series. Non-conservativeness can occur at each of the precipitation partitioning stages: first if $S^*>P$ or $S^*<0$, and second if $U^*>W$ or $U^*<0$. A trial-and-error method is applied to each elementary catchment, the selected α value being the one minimizing the criteria function fc(α) defined as the number of non-conservative annual water balances obtained when calculating S* and U* with α. Incrementation of α is made at steps of 0.01, between -1 and 2, preliminary work having shown that α is never found outside this range with any larger investigated interval. Where a range of α values minimize the criteria function fc(α), the value is selected as the centre of this range.

Ten types of catchments were defined by different IGF influences and corresponding to specific I and α values. Types 1 to 5 are catchments with negative annual water balances (water loss, positive I sign), and with respective α value ranges of [-1; 0],]0; 0.4],]0.4; 0.6[, [0.6; 1[and [1; 2]. Types 6 to 10 are catchments with positive annual water balances (water gain, negative I sign), and with the same α value ranges as types 1 to 5, respectively. Figure 2 shows simplified processes associated with the main values taken by the parameter pair (I, α). Positive I values corresponding to losses are on the left, and negative I values corresponding to gains are on the right. Values of α vary from -1 to 2 from top to bottom.

The choice of a classification into ten types following these α values was driven by the associated hydrological processes, which are specific to each type. First, catchments with α values outside the [0; 1] range exhibit compensating processes. Negative α values correspond to strong IGF affecting the slow-flow component U, associated to opposite direction IGF affecting the quick flow component S. In a similar way, α values comprised between 1 and 2 correspond to strong IGF affecting S, associated to opposite direction IGF affecting U. Second, the catchments with α values inside the [0; 1] range are divided into three groups. Those with α values close to 0 are prone to IGF affecting U and those with α values close to 1 are prone to IGF affecting S. Finally, catchments with α values around 0.5 (from 0.4 to 0.6) are prone to IGF affecting S and U in similar fashion. This results in five groups, each being split in two following the main direction of IGF (gain or loss, depending on the I sign).

In terms of hydrological and hydrogeological processes, outgoing IGF affecting U can be due to diffuse river loss through the riverbed and incoming IGF affecting U can correspond to loss from a neighbouring catchment feeding baseflow. Outgoing IGF affecting S can be due to localized river loss through sinkholes, and incoming IGF affecting S can correspond to loss from a neighbouring catchment activating a karst spring.

[Figure 2]

1.1.3 Hydrograph separation

At each gauging station, daily Q values are filtered in order to separate the quick- and slow-flow components. The slow one is traditionally interpreted as baseflow, which is the part of streamflow corresponding to aquifer drainage. Quick-flow corresponds to surface runoff. In the specific case of karst systems, quick-flow may also include a quick component from the springs that feed the river. Several baseflow separation methods exist; traditional ones are based on graphical analysis, like the fixed-interval, sliding-interval, local-minimum, or Wallingford methods [Gustard et al., 1992; Sloto and Crouse, 1996; Rutledge, 1998; Piggott et al., 2005]. Numerical approaches have also been developed [e.g. Lyne and Hollick, 1979; Eckhardt, 2005]; we used an automation of the one-parameter recursive digital filter proposed by Lyne and Hollick [1979], implemented in the HydRun package [Tang and Carey, 2017]. The filter equation is as follows:

$$S_t = \beta S_{t-1} + \frac{1+\beta}{2}(Q_t - Q_{t-1}) \qquad (9)$$

with S_t and Q_t the filtered quick-flow component and total streamflow at time t, respectively, and β the filter parameter.

We chose this method as it provides consistent results, similar to those obtained with graphical approaches (results not shown). It can easily be automated and has only one β parameter, fixed at 0.91 after a trial-and-error analysis on the studied catchments and considering the results of Nathan and McMahon [1990] on 186 catchments.

1.1.4 Assessment of evapotranspiration

Here, we distinguish between the two terms of actual evapotranspiration E and E*. E is estimated by the standard L'vovich method (Eq. 4) and E* is assessed using independent data time series at a daily time step using three different approaches, in order to provide a range for this component characterized by major uncertainties. The three approaches, respectively based on the methods of Thornthwaite [1948], Dingman [2002], and the GR4J model [Edijatno et al., 1999], are described in Appendix. The final E* value is the mean of those three methods.

1.2 Spatial subdivision and hydro-geomorphologic parameters

1.2.1 Spatial subdivision

The water-balance method described above is applied to the corresponding elementary catchment at each gauging station [Covino et al., 2011; Mallard et al., 2014]. If the station is the most upstream one on the river, the elementary catchment corresponds to the ordinary topographic catchment. Otherwise, the elementary catchment is an intermediate one corresponding to the portion of the basin drained between two gauging stations. For an intermediate catchment, the streamflow Q is calculated as the difference between outlet flow (Q_o) and incoming upstream flow (Q_i, Eq. 10). This is equivalent to considering Q_i and P as the two incoming flows for the intermediate catchment water balance. The S and U components are also obtained from the difference of inputs and outputs (Eqs. 11 and 12). For intermediate catchments, the associated uncertainties are twice as important as those of measured flows.

$$Q = Q_o - Q_i \qquad (10)$$

$$S = S_o - S_i \qquad (11)$$

$$U = U_o - U_i \qquad (12)$$

Several studies [Toth, 1963; Schaller and Fan, 2009; Bouaziz et al., 2018; Fan, 2019] showed the influence of catchment size on IGF. To investigate the scale effect of catchment aggregation on IGF, we analysed the evolution of some hydrological indexes along nested topographic catchments as complementary information. For this, we used the example of the Doubs River basin that has the highest number of successive gauging stations. Results of this analysis are presented in section 4.3.

1.2.2 Hydrological and geomorphological parameters

Hydrological and geomorphological parameters are calculated for studying their correlations at the elementary catchment scale. The studied *hydrological* parameters are:

- S/P and S*/P: part of the quick-flow component normalized by rainfall, obtained without and with IGF compensation, respectively;
- S/Q and S*/Q*: proportion of the quick component within total streamflow, obtained without and with IGF compensation, respectively;
- Q/P and Q*/P: conventional runoff coefficients, obtained without and with IGF compensation, respectively;
- I and |I|: IGF magnitude, respectively considering and ignoring the direction (gain or loss);
- α: relative impact of IGF on surface- and underground flow components.

Since S is obtained from hydrograph separation of daily-data time series, its value is mainly driven by flood events. Thus, S/P and S/Q are good indicators of catchment response after rainfall events, whereas Q/P indicates their global hydrological behaviour.

The *geomorphological* parameters are selected to be representative of the terrain tendency for infiltrating precipitation or producing runoff, and of the potential karstification of underlying geological formations. The computed parameters are the drainage density (ratio of river length to catchment area), the proportion of endorheism (ratio of endorheic areas to catchment area), and the median value of the Index of Development and Persistency of River networks (IDPR) [e.g. Gay et al., 2016]. IDPR is an index quantifying the connectivity of the terrain to the river network, comparing a theoretical river network obtained from thalwegs, and the natural drainage network (see section 2.2.3).

2 Study sites and data sets

2.1 Study sites

The previously described methodology was applied to three regions in France, representing a total area of 25,000 km² (see figure 3 for location and Table 1 for more details). All three regions are totally or partially karstified and have different geological and hydro-meteorological settings. The studied zones belong, from south to north, to the Cévennes Mountains, the Jura Mountains and Normandy.

In the Cévennes region, six drainage basins were studied, including 51 gauging stations. The six are mostly binary karst basins, with head catchments on exposed hardrock receiving around 1500 mm/year precipitation, and downstream parts consisting of limestone plateaux with around 1000 mm/year rainfall.

The Jura Mountains region corresponds to the Doubs River basin, a few kilometres upstream from its confluence with the Saône River and includes 39 gauging stations. Bedrock mostly consists of Jurassic limestone and siltstone that is extensively karstified except in the far northern and western parts of the study area. Precipitation follows a strong elevation gradient, with annual values ranging from 1700 mm in upstream catchments at heights of up to 1400 m a.s.l, to 1200 mm at the outlet at elevations around 200 m a.s.l.

In Normandy, five drainage basins were studied, including 30 gauging stations. The two eastern basins are tributaries of the Seine River, and the other three are coastal basins. The climate is maritime and annual rainfall ranges from 700 to 1000 mm. Rivers of the eastern part of the zone drain chalky limestone with karst covered by clay. The mid-western zone is underlain by Jurassic limestone, corresponding to the western border of the Paris Basin, and the western part overlies the eastern border of the Armorican Massif with older hardrock. Figure 3 shows the twelve drainage basins, with the potential karst aquifers (A) and the gauging station network with karstification of the elementary catchments (B, C, D).

[Table 1]

[Figure 3]

2.2 Data sets

2.2.1 Temporal data

Temporal data used in this paper are as follows (see Table 1 for data time-series periods):

- Daily rainfall, snowfall and potential evapotranspiration depths are from “Safran” (Système d’Analyse Fournissant des Renseignements Atmosphériques à la Neige [Vidal et al., 2010]), edited by the French meteorological service (Météo France);

- Daily streamflow measurements are from the French public streamflow database “Banque Hydro” (http://www.hydro.eaufrance.fr/), managed by the French regional environment directorates (Direction Régionale de l’Environnement, de l’Aménagement et du Logement, DREAL).

Measurement periods may differ between sites but have no significant influence on the results. All hydrological indexes were calculated over different time periods—excluding or including major flood events—and showed similar results, the time series being long enough to be representative of long-term trends.

2.2.2 Spatial data

The spatial data used in this paper are as follows:

- Topographic boundaries of catchments from the French national watersheds database (Base Nationale des Bassins Versants, BNBV) edited by the French central service for hydrometeorology and support on floods prediction (Service Central d’Hydrométéorologie et d’Appui à la Prévision des Inondations, SCHAPI) and the French research institute on science and technology for the environment and agriculture (Institut de Recherche en Sciences et Technologies pour l’Environnement et l’Agriculture, IRSTEA);
- Drainage networks from “BD Carthage” (http://professionnels.ign.fr/bdcarthage), edited by the French geographical institute (Institut Géographique National, IGN);
- Maps of the index of development and persistence of river networks (Indice de Développement et de Persistence des Réseaux, IDPR) from the French geological survey (Bureau de Recherches Géologiques et Minières, BRGM (see next section for more details);

- Map of available soil-water capacity from the French institute of agronomical research (Institut National de la Recherche Agronomique, INRA) [Le Bas, 2018].

2.2.3 Index of development and persistence of river networks (IDPR)

The IDPR was initially developed by the BRGM (French geological survey) for creating simplified groundwater vulnerability maps [Mardhel et al., 2004] at a 25 m spatial resolution. IDPR calculation is based on comparing a theoretical drainage network with the observed natural one. The theoretical network is obtained from a digital elevation model with 25 m spatial resolution, edited by the French Geographical Institute IGN), where thalwegs are theoretical rivers. At each pixel, the IDPR value corresponds to the ratio of the distance to the closest theoretical stream with that to the closest observed stream. Such values range from 0 to 2000. When the observed stream is farther than the theoretical one, the IDPR is low, and vice versa. It is thus representative of the capacity of terrains to be connected to the drainage network.

3 Results

3.1 L'vovich water balance

3.1.1 Application of the initial L'vovich model

Three elementary catchments belonging to the Doubs River basin are taken as examples, to show water-balance results representative of three different configurations of catchments (gaining, losing and conservative). The selected catchments, 1, 2 and 3 on Figure 3, are part of a well-known system of losses of the Doubs River in its upstream part, feeding the Loue

River spring [e.g. Charlier et al., 2014]. Values of water-balance terms for those catchments are provided in a supplementary material.

Figure 4 shows the results of the initial L'vovich annual water-balance method as applied to the 120 elementary catchments. Graphs A and B represent the first-stage partitioning of P into S and W. Most non-karstified elementary catchments fall in the conservative zone (i.e. $0<S<P$ and $0<W<P$), confirming the suitability of this approach for what we consider to be conservative catchments, though some annual water balances for non-karstified catchments fall outside this zone. This shows that they, too, can be affected by IGF, or reflects data uncertainties as raised in section 3.1.1. However, many karstified and mixed elementary catchments fall outside this conservative zone. Some annual S values reach twice the rainfall amount, or are below -1000 mm/yr., indicating that the annual cumulated quick streamflow component between two consecutive gauging stations can either decrease, or increase, by an amount higher than the precipitation over the elementary catchment. This confirms the occurrence of IGF in karstified catchments, highlighting their impact on the quick flow component through either gains or losses. Since W is calculated by the difference of P and S, it also reflects this phenomenon, and can be negative or higher than P, which is physically impossible.

Regarding the second-stage partitioning of precipitation (Fig. 4C,D), the same pattern is seen with karstified elementary catchments falling outside the conservative zone, U values being negative or higher than W. This shows the occurrence of IGF in karstified catchments, which may occur as river loss or groundwater inflow, impacting not only stormflow S but also baseflow U. Consequently, the E term calculated as the difference of W and U (Eq. 2), shows inconsistent annual values, mostly ranging from -4000 to 4000 mm/yr.

[Figure 4]

Application of the initial L'vovich water-balance method to karstified zones sheds light on their hydrological response. It allows identifying the reaches or years with gaining or losing IGFs. It also shows that IGF can affect streamflow in both its quick (S) and slow (U) components. Nevertheless, these first results are insufficient as IGF is not quantified, being integrated into the traditional water-balance terms. This provides unrealistic values of some terms, and especially of evapotranspiration that compensates the non-expressed IGF.

3.1.2 Integration of IGF into the L'vovich model

In order to obtain consistent water balances and to quantify annually the main hydrological processes at the elementary catchment scale, IGF was estimated with Equation 5. Figure 5A shows the cumulative distribution of all 1636 annual I values for the 120 elementary catchments. Despite some years showing IGF magnitudes of several thousands of millimetres, 90% of the annual values range between -1000 and 850 mm, with a median value of 30 mm. Figure 5B shows that, in an I *vs.* Q graph, the points are aligned along the line of equation I = -Q + b, with b corresponding to P-E (Eq. 2), ranging between 0 and 2000 mm/yr. Non-karstified elementary catchments form a group of points defined by Q values ranging between 0 and about 2500 mm/year, and I values ranging between ±-2000 to ±1000 mm/year. Karstified elementary catchments show a broader range of Q values (–2000 to 6000 mm/year), associated with high I values of–4000 to 3000 mm/year, highlighting the specific case of karst catchments where IGF occurs. The order of magnitude of annual IGF being ±1000 mm, it confirms our hypothesis that the potential interannual stock variation of water in the soil reservoir can be neglected compared to IGF. The order of magnitude of the available water capacity in the studied areas is around 100 mm, according to Le Bas [2018].

[Figure 5]

Water-balance terms values obtained with the adapted L'Vovich method are presented in the supplementary material. Are also provided the graphs for the criteria function fc(α), as explained in 1.1.2. Figure 6 shows the adapted L'vovich water-balance graphs, with annual terms corrected by the corresponding estimated IGF values. The quick and slow streamflow components S* and U* are obtained with Equations 7 and 8, and W* is recalculated accordingly. Compared to the initial L'vovich results, P remains the same, whereas E* is now estimated with an independent data time series, as explained in 1.1.4. The first-stage partitioning (Figs. 6A, 6B) shows consistent results, with very few values falling outside the conservative zone, and a limited vertical dispersion, most annual S* and W* values being below 2000 mm/yr. Regarding the second-stage partitioning (Figs. 6C, 6D), E* is quite stable for all elementary catchments (karstified or not), centred on a mean value of 500 mm/yr. U* has variable values from -1000 to 2000 mm/yr, with most non-karstified catchments in the conservative zone.

[Figure 6]

3.2 Relationships between morphometric and hydrological indices

3.2.1 Overview

In order to investigate the relationship between hydrological response and morphological parameters of the catchments, several indices were defined and calculated (see 1.2.2). Each morphometric parameter was plotted as a function of each hydrological index for the 120 elementary catchments, differentiated by the main geology or by geographic location. Global regressions on the 120 catchments gave weak correlations, showing that each site has a hydro-meteorological specificity, as they have very different geological and climatic (Mediterranean, continental/mountainous and oceanic) settings. Operating regressions on catchments grouped by geology slightly increased the correlation strength. The best results were obtained by operating regressions on elementary catchments grouped by geographic location. Table 2 shows the values of obtained determination coefficients (R^2) and p-values for the different linear regressions on catchments grouped by study site.

[Table 2]

Analysis of the correlation coefficient values shows that no systematic correlation exists between investigated parameters, but some trends are visible and significative at a 0.05 probability level. The proportion of endorheism shows no correlation with any of the selected hydrological indexes, and neither relative nor absolute values of I correlate with any geomorphological parameter. Regarding the three defined hydrological indexes, S/P shows the best correlations with drainage density and IDPR, the latter being a slightly better indicator. Use of the terms corrected for I provided better results with higher correlations and at a higher significant level, especially for the S*/P *vs.* IDPR correlation. Generally, the Normandy catchments show the best correlations ($R^2 = 0.52$), and the Jura catchments show the poorest ones (most $R^2 < 0.1$).

Figure 7 shows the scatter plots of S*/P as a function of mean IDPR for the 120 elementary catchments. The determination coefficients are 0.52 for Normandy catchments, 0.22 for Cévennes ones and 0.012 for Jura catchments. The weak correlation for the Jura ones might be explained by the fact that drainage density, in such a purely karstic context, is mostly low, leading to low IDPR values. Gaining and losing catchments mostly have IDPR values <1000, which does not allow a good definition of the hydrological response by IDPR.

[Figure 7]

3.2.2 Relationships between geomorphology and α coefficient

Figure 8 shows the mean pluriannual values of the parameter pair (I, α) for the 120 elementary catchments. Karstified and mixed elementary catchments are slightly more likely to be influenced by important IGF, with a stronger vertical dispersion. More noticeable is the lateral dispersion of karstified and mixed catchments. Though most non-karstified catchments show α values between 0 and 1, several karstified and mixed catchments have α values outside this range. This shows the specificity of karstified catchments as sites of compensating hydrological processes; such processes seem to show a pattern, with low α values associated with positive I values, and high α values associated with negative I values (see Supplementary Material for 3 examples of α in contrasted reaches in the Doubs river). This highlights the fact that IGF losses mostly affect the baseflow component, IGF gains mostly affecting stormflow. It should be noted that α values are chosen as described in section 1.1.2, and that some catchments show a range of satisfying α values. A different selection method might thus lead to slightly modified α values and, locally, to a change in catchment type. Nevertheless, the only arbitrary thresholds are those neighbouring 0.5, where IGF affect both U and S. They have been fixed at 0.4 and 0.6. As shown in Figure 8, karstified, mixt and non-karstified catchments are present in similar proportions in this central zone of the graph. For this reason, different thresholds would not have led to significantly different results.

[Figure 8]

The relationships between α values and geomorphological parameters were investigated as well, showing no significant correlations.

3.2.3 The case of highly karstified catchments

The case of the Jura Mountains catchments seems to be atypical, with no evident relationship between morphological parameters and hydrological indices. This region is well-known to be highly karstified overall. For instance, of all the numerous springs draining the carbonate plateau, the Loue and Lison springs are the third- and the fourth-biggest springs of France, with inter-annual flow of about 10 and 8 m^3/s; at the same time, however, some rivers like the Doubs are known to be totally dry in summer. Figure 9A presents the mean interannual IGF values for each elementary catchment of this zone, showing both positive (orange and red) and negative (light and dark green) values. This means that some catchments are prone to streamflow loss while others gain groundwater. Moreover, the amount of IGF (-1685 to 2860 mm/yr) can be similar to that of precipitation (about 1300-1600 mm/yr), or streamflow.

This can cause poor correlation between the S/P hydrological index and morphological parameters, as the latter probably cannot capture the impact of IGF influence when streamflow is too high.

The southern part of the Jura Mountains presents interesting IGF values, with the strongly deficient Doubs River elementary catchments next to the highly gaining Loue River ones. Figure 9B, a zoom of this region, shows positive artificial tracing tests [surface injection in river losses (sinkholes) and recovery in springs]. It appears that groundwater flow connections highlighted by tracing tests are consistent with the IGF values estimated by pluriannual water balances. Main injection points are in catchments with high IGF values, i.e. groundwater losses, whereas the main restitution points are in elementary catchments with low IGF values, i.e. groundwater gains. Here, they correspond to Doubs River losses feeding the Loue basin via groundwater flow to the Loue spring [Charlier et al., 2014]. This confirms our assumption that IGF is the main cause of non-conservativeness of the studied catchments.

[Figure 9]

4 Discussion

4.1 On the interest of accounting for IGF in the L'vovich model

Accounting for IGF in the L'vovich water-balance allows all its components to have less dispersed and more consistent values, providing reliable results for annual water balances. The new terms S* and U* describe quick surface runoff and slow underground runoff without IGF, respectively, whereas the initial S and U are the quick and slow components of a signal composed of catchment runoff and associated IGF. Yet, some values still fall outside the conservative zones, showing that a better allocation of IGF between quick- and slow flow components is possible, or that other secondary phenomena, such as anthropogenic pressure, may influence the water cycle.

Accounting for IGF in water balances was earlier done by Bouaziz et al. [2018], for example, using the Budyko framework, and showed interesting results in terms of partitioning precipitation into streamflow and evapotranspiration. We have pushed this investigation further, by integrating IGF in the process-based L'vovich model that includes hydrograph decomposition. This allows investigating the influence of IGF on specific hydrological processes, such as stormflow and baseflow. In our case, it showed that IGF affects both stormflow and baseflow in a significant way, notably in a karst aquifer context. Figures 4A and 4B show that many annual S values are "non-conservative" for karst and mixed catchments, meaning that stormflow is affected by incoming or outgoing IGF, even when karst only partially affects the carbonate rocks. Figure 4C also shows inconsistent (negative or several thousands of millimetres) U values, meaning that baseflow in such catchments is affected by incoming or outgoing IGF. Some non-karstified elementary catchments also have baseflow values higher than soil wetting, showing that IGF can occur because of other geological features than karst drains, such as fractured bedrock.

Our method provides a framework for better understanding the influence of IGF on the different hydrological processes. From a perspective of improving the conceptual and digital hydrological models for catchments prone to IGF, it is useful to assess the spatial and temporal variability of IGF, and of its influence on both stormflow and baseflow. Previous work on improving digital modelling of non-conservative catchments [e.g. Le Moine et al., 2007] showed that explicitly accounting for IGF provides better modelling performance than using scaling factors (e.g. scaling of rainfall or catchment surface). Moreover, such work focused on the influence of IGF on the whole streamflow, and not only on its slow and fast components that are often separated in global models. Our approach thus provides an interesting way for improving models that differentiate inflow and outflow from IGF in baseflow or stormflow. It can be applied on a variety of catchments, only requiring standard data sets of rainfall, runoff and evapotranspiration. Regarding regionalization and link with geomorphological indices, we advise to account for the main lithology of catchments, as our results showed that significant differences exist following geology.

4.2 Variability of the hydrology–geomorphology relationship

Our method provides a way of estimating several hydrological parameters obtained from annual water balances. Studied at the elementary catchment scale at the same time as a geomorphological analysis, they allow investigating relationships between hydrological processes and physiographical parameters. Depending upon study sites and investigated parameters, our correlations show strong variability. Weak correlations may be explained by an inability of the geomorphological parameters to describe the diversity of hydrological processes occurring in particular catchments (e.g. extensive karst plateaux), as gains and losses can occur in the same elementary catchment [Charlier et al., 2019]. Nevertheless, some trends provide interesting perspectives in terms of regionalization, in particular when dealing with ungauged basins. These first results could be used, for instance, for identifying gaining and losing areas, for better designing hydrological models structure.

4.3 Water balance and scale effect

Figure 10 shows the evolution of several hydrological indexes (Q/P, I/P, E/P left graph) estimated at gauging stations along the Doubs and Loue rivers–one of its main tributaries–as a function of their distance to outlet. The I/P index represents the interannual IGF depth normalized for P. It globally decreases downstream along the Doubs River, going from 0.5 to nearly 0 at the catchment outlet. The Doubs is thus prone to important streamflow losses (half of annual precipitation), which decrease and tend to zero at the outlet. Regarding the Loue River that collects most of the Doubs River losses (see 3.3.2), at the upstream stations IGF is incoming and represents half of annual precipitation, before decreasing downstream to reach a close-to-equilibrium state at the catchment outlet. This phenomenon is highlighted on the graph and is confirmed by the nearly conservative water balance at the outlet, after the confluence of both rivers. These results agree with Schaller and Fan [2009], who extended the theoretical framework provided by Toth [1963] and found that smaller catchments are more prone to IGF than larger ones, which tend to be more self-containing.

This decrease of groundwater losses along the Doubs is reflected by a higher Q/P index, showing that, from upstream to downstream, a smaller part of precipitation is converted into losses and a greater part goes into streamflow. This is probably slightly limited by the E/P index increasing downstream. The opposite occurs for the Loue River: as IGF gains decrease Q/P also decreases, from 1.5 where IGF gains are important to 0.5 where IGF is small.

The Doubs River has major streamflow losses in its upstream part [e.g. Charlier et al., 2014]; this zone (blue stripes on Fig. 10) clearly affects hydrological indexes as we observe an I/P increase in this zone, showing higher groundwater loss. It also corresponds to a Q/P decrease, streamflow being affected by these losses. The right graph presents the respective proportions of slow U/Q and quick S/Q streamflow components. The loss zone has a specific streamflow signal with an increased S/Q and a decreased U/Q, meaning that the losses affect streamflow mostly in its slow component, i.e. baseflow.

[Figure 10]

Conclusions

We provide a framework for applying traditional annual water balances and adapting them to non-conservative catchments, those that are prone to gains or losses through interbasin groundwater flow, or IGF. Considering that IGF is common in karst catchments and increasingly identified in other geological settings, it is useful to dispose over consistent water balances in catchments prone to groundwater exchange. Such adapted water balances, applied at the elementary catchment scale, allow locating the gaining and losing reaches of streams.

The updated L'vovich model, by separating stormflow and baseflow, allows studying the influence of IGF on both components. Combined with a geological and geomorphological analysis, this approach provides information on the role of physiographical parameters on the occurrence and magnitude of IGF. We show that karst catchments are strongly influenced by IGF, with major impacts on the quick- and slow-flow components of the annual water balance. IGF losses mostly seem to affect the slow-flow component, while IGF gains mostly affect the quick-flow component. Depending on the study sites, significant correlations exist with geomorphological parameters, such as drainage density or IDPR, even if in some cases the latter do not seem to cover all processes involved in IGF.

This innovative approach allows applying consistent water balances over a wide range of natural catchments, including non-conservative highly karstified ones. It provides more reliable results and restores the physical meaning of water balance components in terms of hydrological processes. It also helps hydrologists in making safer interpretations based on annual water budgets, and opens interesting perspectives for the improvement of hydrological models.

Acknowledgements

The work was funded by the French General directorate for risk prevention (Direction Générale de la Prévention des Risques, DGPR) of the Ministry of Ecological and Inclusive Transition, the Central Service for Hydrometeorology and Flood Forecasting (Service Central d'Hydrométéorologie et d'Appui à la Prévision des Inondations, SCHAPI), and the BRGM, French geological survey, France’s reference public sciences organism for Earth Science application in the management of surface and subsurface resources and risks.

References

Andréassian, V., Perrin, C., 2012. On the ambiguous interpretation of the Turc-Budyko nondimensional graph. Water Resources Research 48, https://doi.org/10.1029/2012WR012532

Bailly-Comte, V., Jourde, H., Pistre, S., 2009. Conceptualization and classification of groundwater–surface water hydrodynamic interactions in karst watersheds: Case of the karst watershed of the Coulazou River (southern France). Journal of Hydrology 376, 456–462. https://doi.org/10.1016/j.jhydrol.2009.07.053

Bakalowicz, M., 2005. Karst groundwater: a challenge for new resources. Hydrogeology Journal 13, 148–160. https://doi.org/10.1007/s10040-004-0402-9

Bates, P.D., De Roo, A.P.J., 2000. A simple raster-based model for flood inundation simulation. Journal of Hydrology 236, 54–77. https://doi.org/10.1016/S0022-1694(00)00278-X

Bouaziz, L., Weerts, A., Schellekens, J., Sprokkereef, E., Stam, J., Savenije, H., Hrachowitz, M., 2018. Redressing the balance: quantifying net intercatchment groundwater flows. Hydrology and Earth System Sciences 22, 6415–6434. https://doi.org/10.5194/hess-22-6415-2018

Budyko, M.I., 1974. Climate and life, English ed. / edited by David H. Miller. ed. New York : Academic Press., 508 p.

Carrillo-Rivera, J.J., Cardona, A., Moss, D., 1996. Importance of the vertical component of groundwater flow: a hydrogeochemical approach in the valley of San Luis Potosi, Mexico. Journal of Hydrology 185, 23–44. https://doi.org/10.1016/S0022-1694(96)03014-4

Carrillo-Rivera, J., 2000. Application of the groundwater-balance equation to indicate interbasin and vertical flow in two semi-arid drainage basins, Mexico. Hydrogeology Journal 8, 503–520. https://doi.org/10.1007/s100400000093

Charlier, J.B., Lachassagne, P., Ladouche, B., Cattan, P., Moussa, R., Voltz, M., 2011. Structure and hydrogeological functioning of an insular tropical humid andesitic volcanic watershed: A multi-disciplinary experimental approach. Journal of Hydrology 398, 155–170. https://doi.org/10.1016/j.jhydrol.2010.10.006

Charlier J.B., Desprats J.F., Ladouche B., 2014. Appui au SCHAPI 2014 – Module 1 – Rôle et contribution des eaux souterraines d'origine karstique dans les crues de la Loue à Chenecey-Buillon, Rapport BRGM/RP-63844-FR, 109p.

Charlier, J.B., Ladouche, B., Maréchal, J.C., 2015a. Identifying the impact of climate and anthropic pressures on karst aquifers using wavelet analysis. Journal of Hydrology 523, 610–623. https://doi.org/10.1016/j.jhydrol.2015.02.003

Charlier, J.B., Moussa, R., Bailly-Comte, V., Danneville, L., Desprats, J.F., Ladouche, B., Marchandise, A., 2015b. Use of a flood-routing model to assess lateral flows in a karstic stream: implications to the hydrogeological functioning of the Grands Causses area (Tarn River, Southern France). Environmental Earth Sciences 74, 7605–7616. https://doi.org/10.1007/s12665-015-4704-0

Charlier, J.B., Moussa, R., David, P., Desprats, J., 2019. Quantifying peakflow attenuation/amplification in a karst river using the diffusive wave model with lateral flow. Hydrological Processes. https://doi.org/10.1002/hyp.13472

Chen, Z., Auler, A.S., Bakalowicz, M., Drew, D., Griger, F., Hartmann, J., Jiang, G., Moosdorf, N., Richts, A., Stevanovic, Z., Veni, G., Goldscheider, N., 2017. The World Karst Aquifer Mapping project: concept, mapping procedure and map of Europe. Hydrogeology Journal 25, 771–785. https://doi.org/10.1007/s10040-016-1519-3

Covino, T., McGlynn, B., Mallard, J., 2011. Stream-groundwater exchange and hydrologic turnover at the network scale. Water Resources Research 47. https://doi.org/10.1029/2011WR010942

Dingman S.L., 2002. Physical Hydrology, pp. 575, Waveland Press, 2nd edition, ISBN: 978-1-57766-561-8

Eakin, T.E., 1966. A regional interbasin groundwater system in the White River Area, southeastern Nevada. Water Resources Research 2, 251–271. https://doi.org/10.1029/WR002i002p00251

Eckhardt, K., 2005. How to construct recursive digital filters for baseflow separation. Hydrological Processes 19, 507–515. https://doi.org/10.1002/hyp.5675

Edijatno, De Oliveira Nascimento, N., Yang, X., Makhlouf, Z., Michel, C., 1999. GR3J: a daily watershed model with three free parameters. Hydrological Sciences Journal 44, 263–277. https://doi.org/10.1080/02626669909492221

Fan, Y., 2019. Are catchments leaky? Wiley Interdisciplinary Reviews: Water 6. https://doi.org/10.1002/wat2.1386

Gay, A., Cerdan, O., Mardhel, V., Desmet, M., 2016. Application of an index of sediment connectivity in a lowland area. Journal of Soils and Sediments 16, 280–293. https://doi.org/10.1007/s11368-015-1235-y

Genereux, D.P., Wood, S.J., Pringle, C.M., 2002. Chemical tracing of interbasin groundwater transfer in the lowland rainforest of Costa Rica. Journal of Hydrology 258, 163–178. https://doi.org/10.1016/S0022-1694(01)00568-6

Genereux, D.P., Jordan, M.T., Carbonell, D., 2005. A paired-watershed budget study to quantify interbasin groundwater flow in a lowland rain forest, Costa Rica. Water Resources Research 41. https://doi.org/10.1029/2004WR003635

Genereux, D.P., Jordan, M., 2006. Interbasin groundwater flow and groundwater interaction with surface water in a lowland rainforest, Costa Rica: A review. Journal of Hydrology 320, 385–399. https://doi.org/10.1016/j.jhydrol.2005.07.023

Gustard, A., Bullock, A., Dixon, J.M., 1992. Low flow estimation in the United Kingdom, Report / Institute of Hydrology. Institute of Hydrology, Wallingford

Laaha, G., Blöschl, G., 2006. Seasonality indices for regionalizing low flows. Hydrological Processes 20, 3851–3878. https://doi.org/10.1002/hyp.6161

Ladouche, B., Marechal, J.C., Dorfliger, N., 2014. Semi-distributed lumped model of a karst system under active management. Journal of Hydrology 509, 215–230. https://doi.org/10.1016/j.jhydrol.2013.11.017

Le Bas, C., 2018. Carte de la Réserve Utile en eau issue de la Base de Données Géographique des Sols de France. https://doi.org/10.15454/JPB9RB

Le Moine, N., Andréassian, V., Perrin, C., Michel, C., 2007. How can rainfall-runoff models handle intercatchment groundwater flows? Theoretical study based on 1040 French catchments. Water Resources Research 43. https://doi.org/10.1029/2006WR005608

Lebecherel, L., Andréassian, V., Perrin, C., 2013. On regionalizing the Turc-Mezentsev water balance formula. Water Resources Research 49, 7508–7517. https://doi.org/10.1002/2013WR013575

López-Chicano, M., Calvache, M.L., Martín-Rosales, W., Gisbert, J., 2002. Conditioning factors in flooding of karstic poljes—the case of the Zafarraya polje (South Spain). CATENA 49, 331–352. https://doi.org/10.1016/S0341-8162(02)00053-X

Lvovich, M.I., 1979. World water resources, present and future. GeoJournal 3, 423–433. https://doi.org/10.1007/BF00455981

Lyne, V., Hollick, M., 1979. Stochastic time-variable rainfall-runoff modelling, I., E. Aust. Natl. Conf. Publ. 79/10, 89-93,Inst.of Eng., Aust., Canberra, 1979.

Mallard, J., McGlynn, B., Covino, T., 2014. Lateral inflows, stream-groundwater exchange, and network geometry influence stream water composition. Water Resources Research 50, 4603–4623. https://doi.org/10.1002/2013WR014944

Mardhel, V., Frantar P., Uhan J., Miso A., 2004. Index of development and persistence of the river networks as a component of regional groundwater vulnerability assessment in Slovenia. International conference on groundwater vulnerability assessment and mapping, Ustron, Poland, 15-18 June 2004

Maréchal, J.C., Ladouche, B., Dörfliger, N., 2008. Karst flash flooding in a Mediterranean karst, the example of Fontaine de Nîmes. Engineering Geology 99, 138–146. https://doi.org/10.1016/j.enggeo.2007.11.013

Mayaud, C., Gabrovšek, F., Blatnik, M., Kogovšek, B., Petrič, M., Ravbar, N., 2019. Understanding flooding in poljes: A modelling perspective. Journal of Hydrology 575, 874–889. https://doi.org/10.1016/j.jhydrol.2019.04.092

Moussa, R., Bocquillon, C., 2009. On the use of the diffusive wave for modelling extreme flood events with overbank flow in the floodplain. Journal of Hydrology 374, 116–135. https://doi.org/10.1016/j.jhydrol.2009.06.006

Nathan, R.J., McMahon, T.A., 1990. Evaluation of automated techniques for base flow and recession analyses. Water Resources Research 26, 1465–1473. https://doi.org/10.1029/WR026i007p01465

Pellicer-Martínez, F., Martínez-Paz, J.M., 2014. Assessment of interbasin groundwater flows between catchments using a semi-distributed water balance model. Journal of Hydrology 519, 1848–1858. https://doi.org/10.1016/j.jhydrol.2014.09.067

Piggott, A.R., Moin, S., Southam, C., 2005. A revised approach to the UKIH method for the calculation of baseflow / Une approche améliorée de la méthode de l'UKIH pour le calcul de l'écoulement de base. Hydrological Sciences Journal 50. https://doi.org/10.1623/hysj.2005.50.5.911

Ponce, V.M., Shetty, A.V., 1995. A conceptual model of catchment water balance: 1. Formulation and calibration. Journal of Hydrology 173, 27–40. https://doi.org/10.1016/0022-1694(95)02739-C

Rutledge, A.T., 1998. Computer programs for describing the recession of ground-water discharge and for estimating mean ground-water recharge and discharge from streamflow records-update. https://doi.org/10.3133/wri984148

Schaller, M.F., Fan, Y., 2009. River basins as groundwater exporters and importers: Implications for water cycle and climate modeling. Journal of Geophysical Research 114. https://doi.org/10.1029/2008JD010636

Sivapalan, M., Yaeger, M.A., Harman, C.J., Xu, X., Troch, P.A., 2011. Functional model of water balance variability at the catchment scale: 1. Evidence of hydrologic similarity and space-time symmetry. Water Resources Research 47. https://doi.org/10.1029/2010WR009568

Sloto, R.A., Crouse, M.Y., 1996. HYSEP: A computer program for streamflow hydrograph separation and analysis. https://doi.org/10.3133/wri964040

Tang, W., Carey, S.K., 2017. HydRun: A MATLAB toolbox for rainfall-runoff analysis. Hydrological Processes 31, 2670–2682. https://doi.org/10.1002/hyp.11185

Thiéry D., 2014. Logiciel GARDÉNIA, version 8.2. Guide d'utilisation. Rapport BRGM/RP-62797-FR, update: Mai 2015.

Thornthwaite, C.W., 1948. An approach toward a rational classification of climate. Geographical Review 38, 55–94. https://doi.org/10.2307/210739

Thyne, G.D., Gillespie, J.M., Ostdick, J.R., 1999. Evidence for interbasin flow through bedrock in the southeastern Sierra Nevada. Geological Society of America Bulletin 111, 1600. https://doi.org/10.1130/0016-7606(1999)111<1600:EFIFTB>2.3.CO;2

Tóth, J., 1963. A theoretical analysis of groundwater flow in small drainage basins. Journal of Geophysical Research 68, 4795–4812. https://doi.org/10.1029/JZ068i016p04795

Vidal, J.P., Martin, E., Franchistéguy, L., Baillon, M., Soubeyroux, J.M., 2010. A 50-year high-resolution atmospheric reanalysis over France with the Safran system. International Journal of Climatology 30, 1627–1644. https://doi.org/10.1002/joc.2003

List of variables

Symbol	Unit	Description
P	mm/yr	Precipitations (solid and liquid)
Q	mm/yr	Total specific river streamflow (per surface unit)
Q*	mm/yr	Specific runoff (part of streamflow fed by the elementary catchment)
S	mm/yr	Specific surface runoff (quick flow component), including IGF
S*	mm/yr	Specific surface runoff (quick flow component), excluding IGF
U	mm/yr	Underground specific runoff (slow flow component), including IGF
U*	mm/yr	Underground specific runoff (slow flow component), excluding IGF
W	mm/yr	Wetting (part of precipitations not feeding surface runoff), including IGF
W*	mm/yr	Wetting (part of precipitations not feeding surface runoff), excluding IGF
E	mm/yr	Evapotranspiration calculated as per L'vovich initial water balance
E*	mm/yr	Evapotranspiration estimated by modelling
I	mm/yr	Interbasin groundwater flow (<0 for gains and >0 for losses)

Appendix: Estimation of evapotranspiration

E* is estimated at a daily time step using three different approaches, so as to provide a range to this component characterized by major uncertainties. The three approaches are based on the water-budget methods proposed by Thornthwaite [1948] and Dingman [2002], and by Edijatno et al. [1999] for the GR4J lumped model. All three consider soil as a reservoir, used for distributing the input (precipitation) into evapotranspiration and effective rainfall.

In the Thornthwaite [1948] method, water in the soil reservoir is directly available for evapotranspiration, and precipitation produces effective rainfall (P_{eff}) only after soil saturation. The following algorithm summarizes the method:

- If P <E0, the difference E0 – P is subtracted from the soil-water stock C until it is empty:
  - $C_t = max\,(0\,;\, C_{t-1} + P_t - E0_t)$
  - $E_t = min\,(E0_t\,;\, C_{t-1} + P_t)$
  - $P_{efft} = 0$
- If P >E0, the difference P – E0 first feeds the soil-water stock C and then produces efficient rainfall:
  - $C_t = min\,(C_{max}\,;\, C_{t-1} + P_t - E0_t)$
  - $E_t = E0_t$
  - $P_{efft} = max\,(0\,;\, C_t + P_t - E0_t - C_{max})$

The Dingman [2002] method is similar to the previous one, with an exponential law governing water extraction for evapotranspiration from the soil reservoir:

- If P <E0, the difference E0 – P is subtracted from the soil water stock C following an exponential law:
  - $C_t = C_{t-1} \cdot e^{\frac{-(E0_t - P_t)}{C_{max}}}$
  - $E_t = P_t + C_{t-1} - C_t$
  - $P_{efft} = 0$
- If P >E0, the difference P – E0 first feeds the soil-water stock C and then produces efficient rainfall (as in the Thornthwaite method):
  - $C_t = min\,(C_{max}\,;\, C_{t-1} + P_t - E0_t)$
  - $E_t = E0_t$
  - $P_{efft} = max\,(0\,;\, C_t + P_t - E0_t - C_{max})$

The GR method is derived from the GR hydrological models [Edijatno et al., 1999] and involves a quadratic law for the water-level variation in the soil reservoir. The algorithm, summarized below, then was adapted to the BRGM ‘Gardenia’ model [Thiéry, 2014], which has been used here.

- If P <E0, the difference $E_n = E0 - P$ is subtracted from the soil-water stock C, following a quadratic law:
    - $dC = \left((C/C_{max})^2 - 2(C/C_{max})\right) \cdot dE_n$
    - $dE_t = -dC$
    - $P_{eff} = 0$
- If P >E0, the difference $P_n = P - E0$ is partitioned into effective rainfall and soil storage following a quadratic law:
    - $dC = (1 - (C/C_{max})^2) \cdot dP_n$
    - $E = E0$
    - $dP_{eff} = (C/C_{max})^2 \cdot dP_n$
- Integration of the differential variations provides expressions of C_t, E_t and P_{efft} as a function of C_{t-1}, C_{max}, and $\tanh(E_n/C_{max})$ or $\tanh(P_n/C_{max})$.

The final E* value corresponds to the mean of the three estimation method results.

Tables

	Study zone area (km²)	Gauging stations	Median gauged area (km²)	Time series length
Ardèche	2257	9	193	1996 - 2014
Cèze	1048	6	192	2002 - 2011
Gardons	1853	10	137	2008 - 2014
Vidourle	772	4	182	2009 - 2014
Hérault	2203	9	223	2007 - 2014
Tarn	2145	13	64	1984 - 2014
Total Cévennes	10300	51	172	8 years (median)
Doubs	7400	39	121	1998 - 2014
Total Jura	7400	39	121	16 years (median)
Iton	1048	2	524	1999 - 2014
Risle	1803	5	84	2001 - 2014
Touques	800	5	106	2010 - 2014
Dives	879	6	113	2009 - 2014
Orne	2260	12	127	2005 - 2014
Total Normandy	6800	30	127	9 years (median)
Total all basins	24500	120	145	9 years (median)

Table 1: Studied catchments and associated available data

	Study zone	S/P	S/Q	Q/P	S*/P	S*/Q*	Q*/P	I	|I|
IDPR	Normandy	0.22^b	0.30^b-	-	**0.52^a**	**0.41^a**	**0.46^a**	-	-
	Cevennes	0.10^c	-	-	0.22^a	0.12^c	0.19^b	-	-
	Jura	0.11^c		0.12^c	-	-	-	0.10^c	-
Drainage density	Normandy	0.20^c	0.20^c	-	**0.46^a**	0.36^b	**0.52^a**	-	-
	Cevennes	0.11^c	-	-	0.14^c	-	0.12^c	-	-
	Jura	-	-	-	-	-	-	-	-
Endorheism	Normandy	-	-	-	-	-	-	-	-
	Cevennes	-	-	-	-	-	0.11^c	-	-
	Jura	-	-	-	-	-	-	-	-

Table 2: Synthesis of R^2 values for all geomorphological and hydrological parameters. Values are obtained from linear regressions for elementary catchments in the three study areas: Normandy, Cévennes and Jura. ^{a}, ^{b}, and ^{c} indicates whether the correlation is statistically significant (non-significant probability level of 0.001, 0.01, and 0.05, respectively). R^2 values above 0.4 are shown in bold. R^2 values below 0.1 and with non-significant probability level higher than 0.05 are shown as dashes.

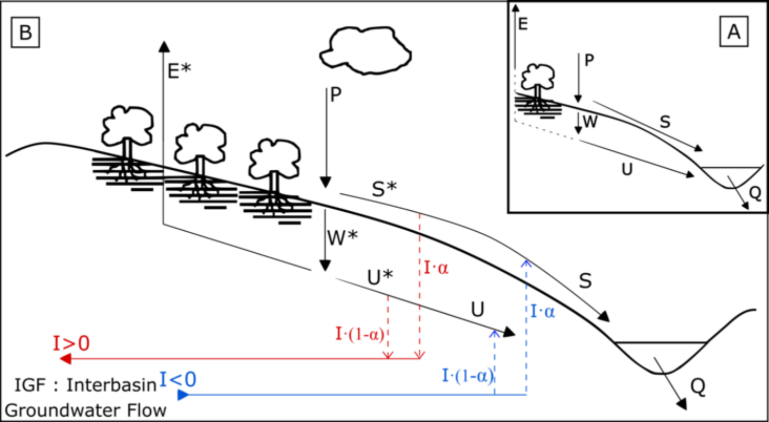

B
A
E*
P
S*
W*
U*
U
S
Q
I·α
I·(1-α)
I>0
I<0
IGF : Interbasin
Groundwater Flow
E
P
W
S
U
Q

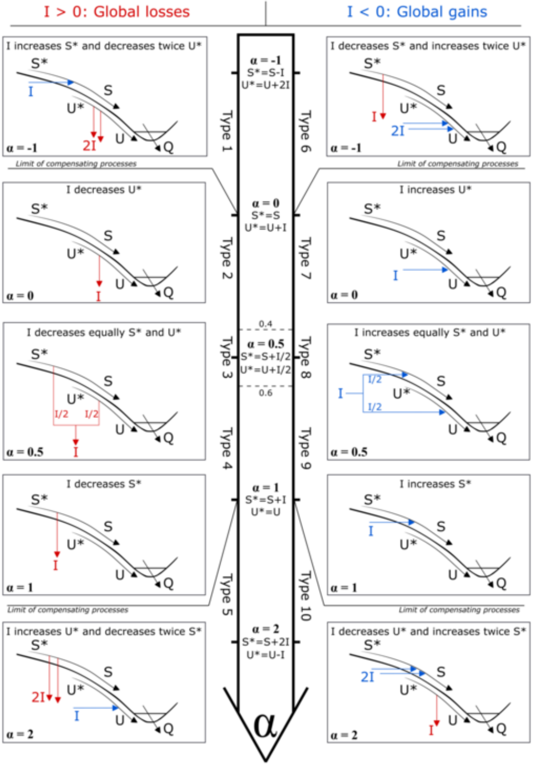

I > 0: Global losses
I < 0: Global gains
I increases S* and decreases twice U*
α = -1
Limit of compensating processes
I decreases U*
α = 0
I decreases equally S* and U*
α = 0.5
I decreases S*
α = 1
I increases U* and decreases twice S*
α = 2
I decreases S* and increases twice U*
I increases U*
I increases equally S* and U*
I increases S*
I decreases U* and increases twice S*
α = -1
S*=S-I
U*=U+2I
α = 0
S*=S
U*=U+I
0.4
α = 0.5
S*=S+I/2
U*=U+I/2
0.6
α = 1
S*=S+I
U*=U
α = 2
S*=S+2I
U*=U-I
Type 1
Type 2
Type 3
Type 4
Type 5
Type 6
Type 7
Type 8
Type 9
Type 10
α

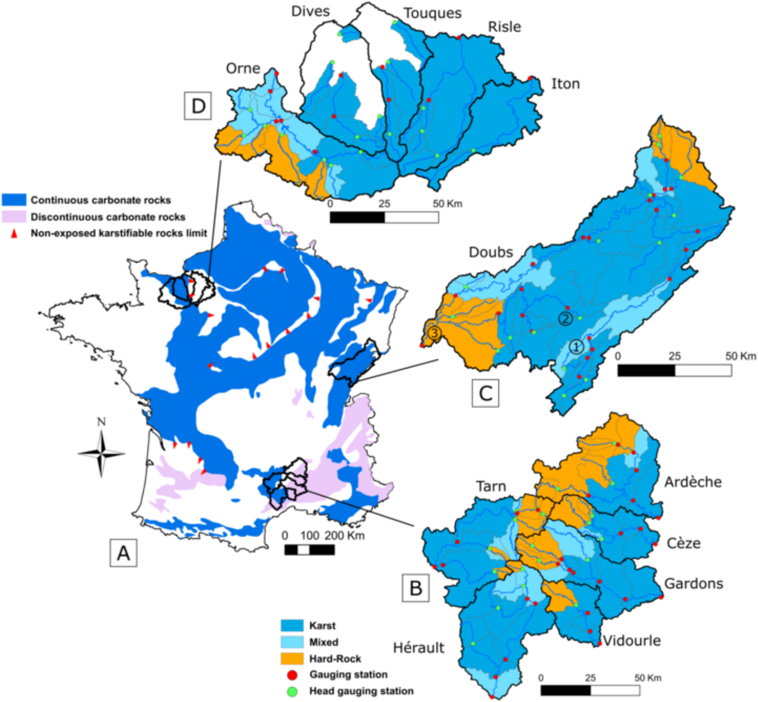

Dives
Touques
Risle
Orne
Iton
D
0
25
50 Km
Continuous carbonate rocks
Discontinuous carbonate rocks
Non-exposed karstifiable rocks limit
Doubs
2
1
3
0
25
50 Km
C
N
0
100
200 Km
A
Tarn
Ardèche
Cèze
Gardons
B
Vidourle
Hérault
Karst
Mixed
Hard-Rock
Gauging station
Head gauging station
0
25
50 Km

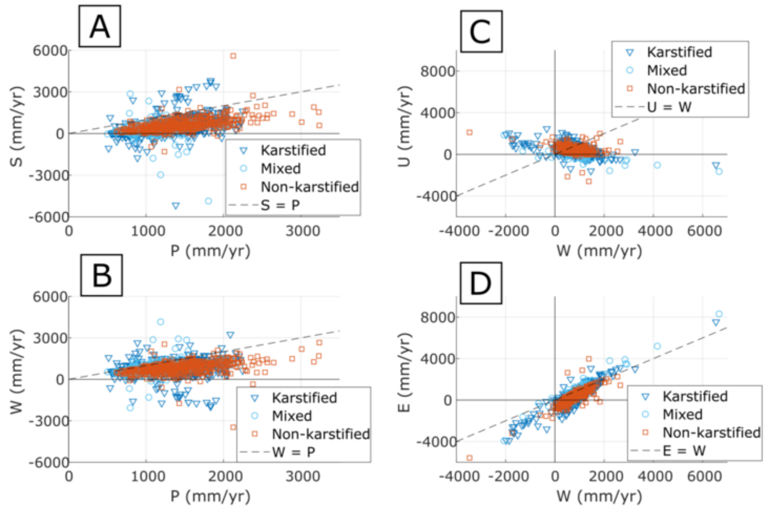
A
B
C
D
S (mm/yr)
W (mm/yr)
U (mm/yr)
E (mm/yr)
P (mm/yr)
W (mm/yr)
6000
3000
0
-3000
-6000
8000
4000
-4000
1000
2000
-2000
Karstified
Mixed
Non-karstified
S = P
W = P
U = W
E = W

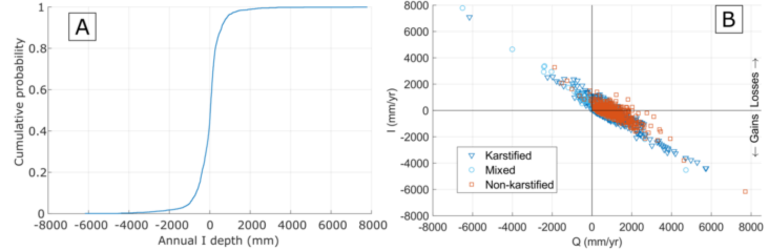

A
Cumulative probability
Annual I depth (mm)
B
I (mm/yr)
Q (mm/yr)
Losses →
← Gains
Karstified
Mixed
Non-karstified

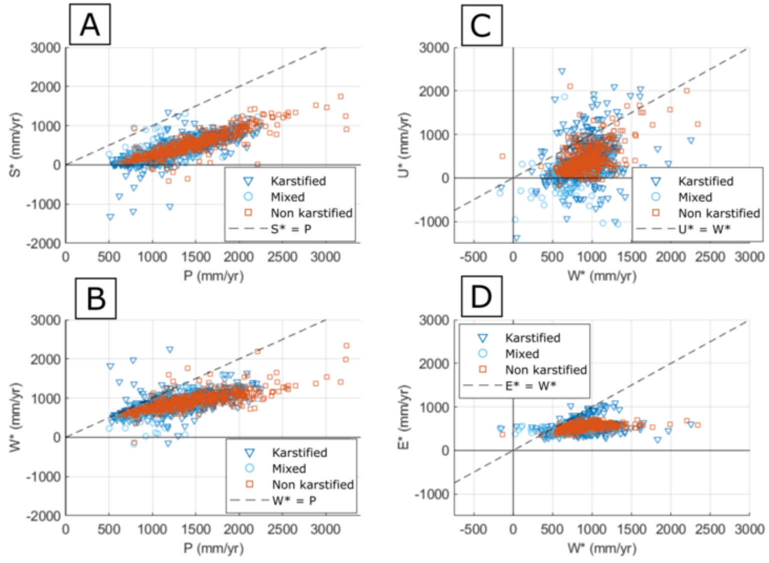

A
S* (mm/yr)
P (mm/yr)
Karstified
Mixed
Non karstified
S* = P
B
W* (mm/yr)
P (mm/yr)
Karstified
Mixed
Non karstified
W* = P
C
U* (mm/yr)
W* (mm/yr)
Karstified
Mixed
Non karstified
U* = W*
D
E* (mm/yr)
W* (mm/yr)
Karstified
Mixed
Non karstified
E* = W*

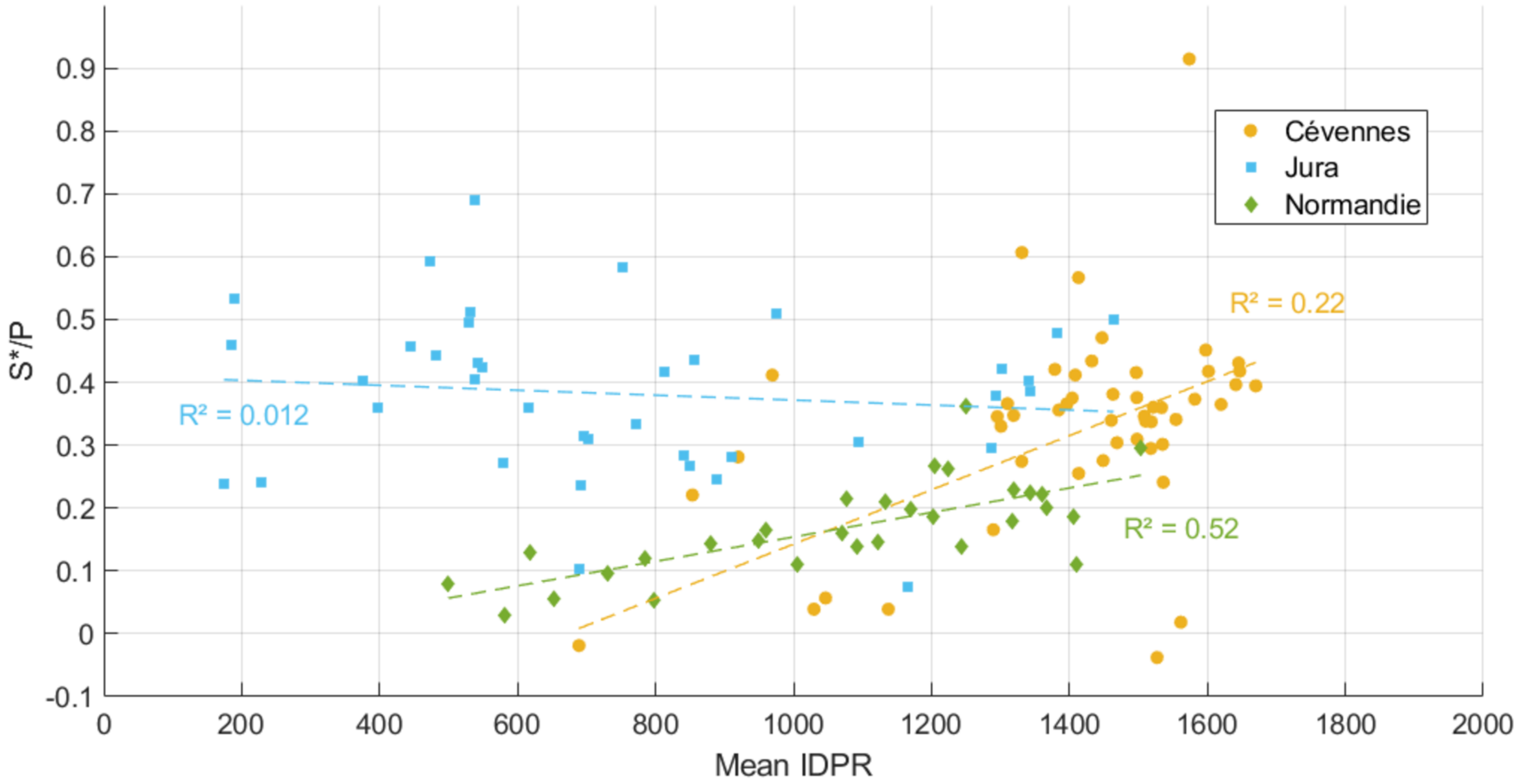

Cévennes
Jura
Normandie
R² = 0.22
R² = 0.012
R² = 0.52
S*/P
Mean IDPR
0.9
0.8
0.7
0.6
0.5
0.4
0.3
0.2
0.1
0
-0.1
0
200
400
600
800
1000
1200
1400
1600
1800
2000

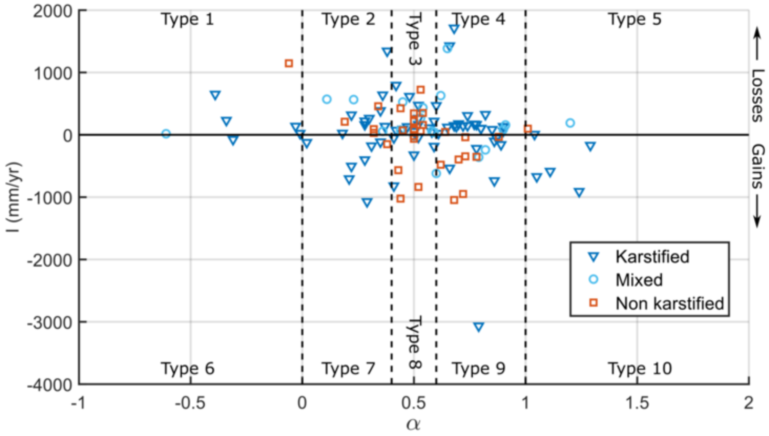

Type 1
Type 2
Type 3
Type 4
Type 5
Type 6
Type 7
Type 8
Type 9
Type 10
Losses
Gains
I (mm/yr)
α
2000
1000
0
-1000
-2000
-3000
-4000
-1
-0.5
0
0.5
1
1.5
2
Karstified
Mixed
Non karstified

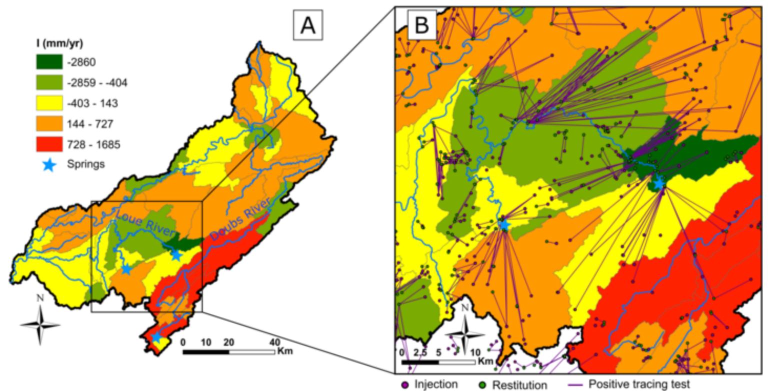
A
I (mm/yr)
-2860
-2859 - -404
-403 - 143
144 - 727
728 - 1685
Springs
Loue River
Doubs River
N
0 10 20 40
Km
B
N
0 2,5 5 10
Km
Injection
Restitution
Positive tracing test

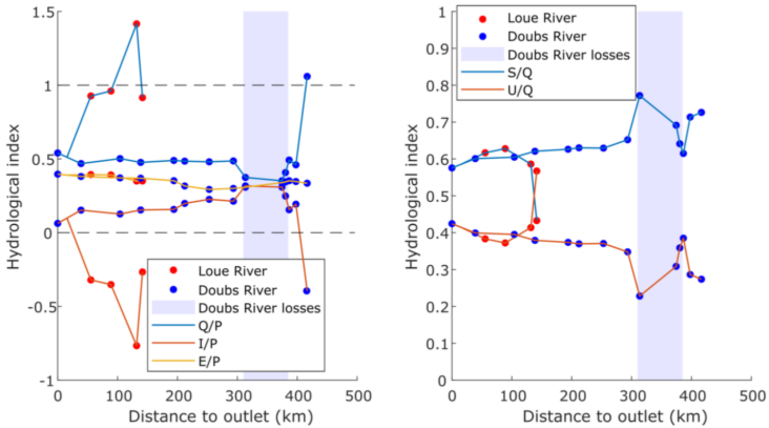

Hydrological index
Distance to outlet (km)
Loue River
Doubs River
Doubs River losses
Q/P
I/P
E/P
S/Q
U/Q

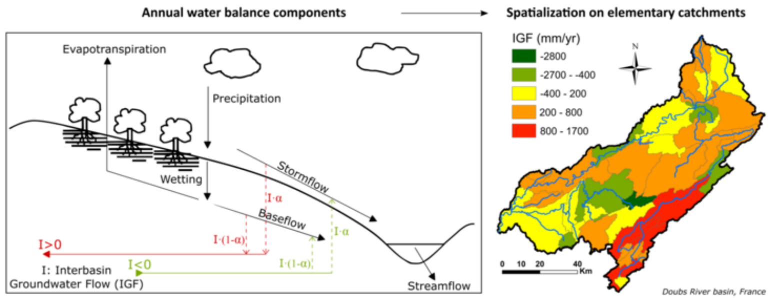

Annual water balance components
Spatialization on elementary catchments
Evapotranspiration
Precipitation
Wetting
Stormflow
Baseflow
I·α
I·(1-α)
I·α
I·(1-α)
I>0
I<0
I: Interbasin
Groundwater Flow (IGF)
Streamflow
IGF (mm/yr)
-2800
-2700 - -400
-400 - 200
200 - 800
800 - 1700
N
0 10 20 40
Km
Doubs River basin, France